RSC Advances

ROYAL SOCIETY OF CHEMISTRY

www.rsc.org/advances

RSCPublishing

ARTICLE

Partially embedded gold nanoislands in a glass substrate for SERS applications

Mohammad Tariq Yaseen[abc], Minfeng Chen[c], and Yia-Chung Chang[cd*]

We investigate the surface enhanced Raman scattering (SERS) of biomolecules attached to partially embedded gold nanoislands in a transparent substrate. In order to generate SERS hot spots in a large area, partially-embedded gold nanoislands were fabricated via thermal annealing of a thin gold layer. The partially embedded gold nanoislands have average sizes varying from 10 nm to 50nm. The SERS performance has been investigated for samples made with various thicknesses of gold thin film. The SERS spectra showed that gold thin film with 4.5nm initial thickness can produce the highest SERS signal due to the high density of uniform partially embedded gold nanoislands with average size around 22nm. Furthermore, we perform numerical simulations based on rigorous coupled-wave analysis (RCWA) and finite difference time domain (FDTD) to show that the SERS enhancement is originated from enhanced electric fields surrounding the partially embedded gold nanoislands. Hence, we have demonstrated a simple, stable, large-area, and low cost preparation process for producing SERS platform with excellent sensitivity for biosensing.

Introduction

Controlling the nanostructure morphology is technologically important, since it can tune the essential chemical and physical properties of the materials. For example, gold and silver nanoparticles have attracted substantial interest in various fields because of their interesting optical properties attributed to their surface plasmon resonance, which depend on their size and shape. Because of their unique scattering and absorption properties compared with conventional bulk metal materials, gold and silver nanoparticles have been used in many applications, for instance, biosensing[1], and surface-enhanced Raman scattering (SERS).[2]

SERS is considered as one of the most powerful analytical tools in the biological and chemical research for understanding molecular information such as chemical bonding, composition and crystal orientation[3]. The fundamental physics of SERS is based on inelastic scattering of molecules caused by the excitation of various vibrational modes and then the Raman signal is greatly enhanced by localized surface plasmon resonance (LSPR) induced by the metallic surface. Then molecular information can be recognized accurately according to the frequency shifts in the Raman spectrum.[4,5]

[a]*Department of Engineering and System Science, NTHU, Hsinchu 300, Taiwan*
[b]*Nano Science and Technology Program, Taiwan International Graduate Program, Academia Sinica, Taipei 115, Taiwan*
[c]*Research Centre for Applied Sciences, Academia Sinica, Taipei, 115 Taiwan*
[d]*Department of Physics, National Cheng Kung University, Tainan, 701 Taiwan*
* E-mail: *yiachang@gate.sinica.edu.tw*

Because of the swift growth in nanoplasmonics[6] and the impact of optical detection of single molecules at room temperature using surface-enhanced Raman scattering[7] well-developed nanofabrication tools have been used recently to produce various types of metallic nanostructures as SERS-active substrates to enhance the electromagnetic field, including bow-tie nanostructues obtained via nanosphere lithography,[8] nanohole and nanodisk arrays[9] and other patterns obtained by e-beam lithography,[10] naturally formed rough metals surfaces, and colloidal metallic nanoparticles.[11-14] Different methods were used to synthesize metallic nanostructures in glass, for example, ion exchange,[15,16] direct ion implantation,[17] and sol-gel methods.[18]

In this work, partially embedded gold nanoislands in glass were investigated as SERS-active substrates. Gold nanoislands can be formed, partially embedded, and tuned in glass by thermal annealing. Thermal annealing technique provides a low cost nanostructure fabrication. Also, it can be controlled to produce closely packed metallic nanoislands, which can generate a higher local field and a stronger SERS effect than isolated particles.

The density and the localized surface plasmon resonance wavelength of the gold nanoislands can be tuned by varying the initial thickness and the annealing process.[19,20] However, simple, reliable, efficient, cost-effective, and tunable techniques such as thermal annealing are required to produce large scale, low cost, reproducible SERS substrates that can be integrated

with optics devices in order to meet the growing interest in potential SERS applications such as biosensing.

We used the SEM and AFM to characterize the morphology of the annealed gold thin films on glass with thickness varying from 1.5 to 5.5 nm. We characterized the prepared SERS substrates before and after annealing by various instruments to analyse the structural and optical properties of the synthesized nanoislands. Field emission scanning electron microscope (FE-SEM) images of the nanoislands were determined using a FEI Nova200 FE-SEM operated at 10kV. The SERS activity of the proposed substrate was examined by using 4-Mercaptobenzoic acid (p-MBA) and Rhodamine 6G (R6G) as probing adsorbents. Raman spectra were obtained with a Jobin Yvon LabRam HR 800 micro-Raman spectrometer equipped with a microscope (Panasonic Super Dynamic). A 632.8nm Helium-Neon laser was used as the excitation source. The Raman band of a silicon wafer at 520cm^{-1} was used to calibrate the spectrometer. Spectroscopic ellipsometry (SE) measurements were done by VASE-Ellipsometry (J.A. Woollam) .The UV/vis absorption spectra were obtained using a V-630 UV/vis spectrophotometer.

We found that gold thin film with 4.5 nm initial thickness can achieve the highest SERS intensity. Finally, Numerical simulations based on rigorous coupled-wave analysis (RCWA) [21] and finite difference time domain (FDTD)[22] were carried out for two cases to evaluate the electromagnetic field for the partially embedded gold nanoislands and comparing the results with free-standing single Au spheres on a substrate. The proposed SERS substrates feature in simple fabrication process, cost-effective, high field enhancement, large uniform area that could be a good candidate for biosensing.

Experimental Results

The gold films with initial thickness of 1.5, 2.5, 3.5, 4.5, and 5.5nm were deposited on clean glass substrates using e-gun evaporator (AST, Taiwan) at a deposition rate of 0.1 Å/sec. The thickness was determined by the spectroscopic ellipsometry measurements. After that, the samples were put inside the oven for thermal annealing at 550 ^{0}C, which is close to the glass transition temperature.

After the thermal annealing, gold nanoislands are formed with diameters around tens of nanometers. The initial thickness of the gold thin film and the annealing temperature determine the final surface morphology of the gold nanoislands, as shown in Fig. 1. Since the gold thin films were annealed at near glass transition temperature, the gold nanoislands will be partially embedded in the glass substrate.

The origin of the light absorption by gold nanostructures is the coherent oscillation of the conduction band electrons induced by the interaction with the electromagnetic field. This effect is generally known as surface plasmon resonance (SPR) or localized surface plasmon resonance (LSPR) depending on the shape of the gold nanostructure; and this effect is absent in the individual atoms and bulk form.

Fig. 2(a) shows the absorption spectra of the gold thin films, which were measured using UV-Vis spectrometer. It shows broader absorption spectra and higher light absorption at thicker films. The absorption peak wavelength shifts to longer wavelength when the thickness increases, as shown in Fig. 2(b). Fig. 2(c) shows the absorption spectra of gold nanoislands of different samples, whose morphologies are shown in Fig. 1. The light absorption is higher for gold nanoislands and absorption peaks are narrower compared to the corresponding

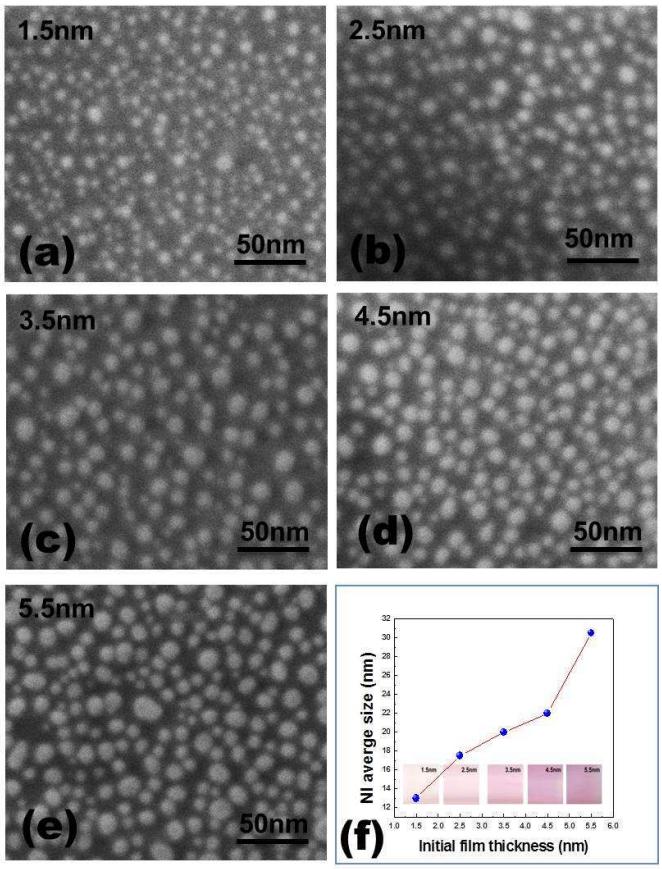

Fig. 1 (a-e) The SEM images of the thermally annealed gold thin films with different initial thicknesses. (f) The estimated average size of the nanoislands of each sample.

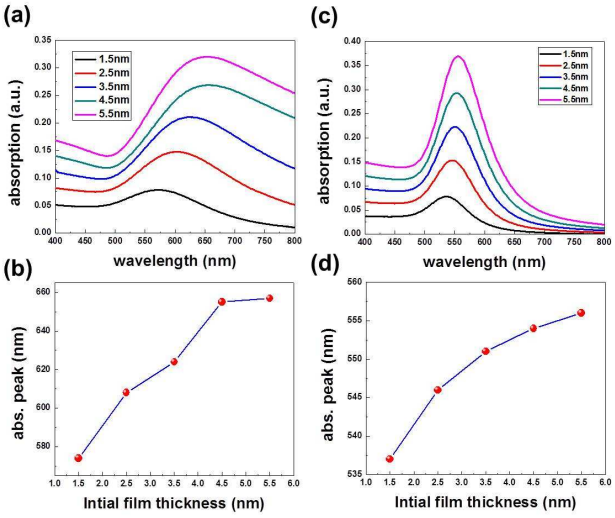

Fig. 2. (a) UV−vis extinction spectra of gold thin films with various thicknesses before thermal annealing. (b) Absorption peak position of gold thin films before thermal annealing as a function of thickness. (c) UV−vis extinction spectra of the thermally annealed gold thin films with various thicknesses. (d) Absorption peak position of thermally annealed gold thin films as a function of thickness.

gold thin films. The absorption peak wavelength as a function of initial film thickness is shown in Fig. 2(d). The peak position shifts to longer wavelength as the film thickness increases.

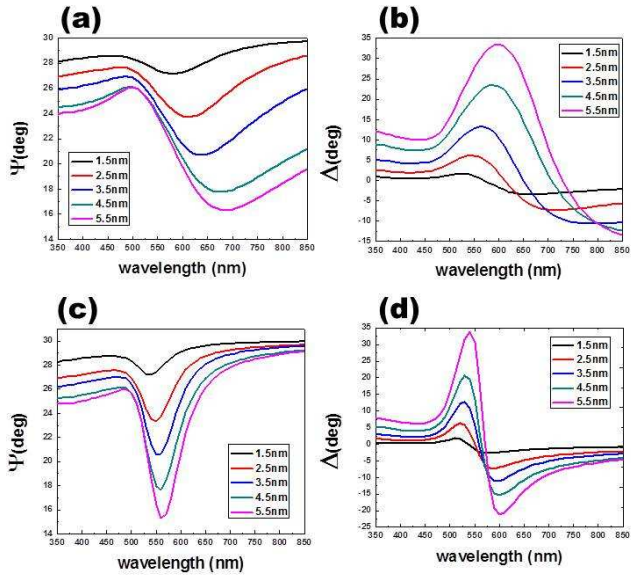

Fig. 3. (a,b) SE signals of gold thin films with various thicknesses before thermal annealing. (c,d) SE signals of thermally annealed gold thin films with various thicknesses.

Fig. 3 shows the spectral response of the SE signals (Ψ and Δ) of the gold films with initial thickness 1.5, 2.5, 3.5, 4.5, and 5.5nm before and after the thermal annealing. The spectral response of Ψ and Δ was also used to confirm the formation of gold nanoislands on the glass substrate after thermal annealing of the gold thin film. The SE signals (Ψ and Δ) are very sensitive to any change in the surface morphology, thickness, and optical index of the measured sample. Fig. 3(a) and (b) show the (Ψ and Δ) spectra of the gold thin film before the thermal annealing. Fig. 3(c) and (d) show the change in Ψ and Δ spectra due to the change in surface morphology of the gold thin film after thermal annealing.

After thermal annealing, there is a clear dip around 560nm in the Ψ spectra [see Fig. 3(c)] and a sign change in Δ spectra [see Fig. 3(d)], in strong contrast to the response before thermal annealing. This change in SE signals of the prepared sample before and after annealing can be attributed to the change in the surface morphology due to formation of gold nanoislands after thermal annealing, which leads to localized surface plasmon resonance (LSPR).

From SE measurements of the unannealed and annealed samples, we obtained the dielectric index (ε_1, ε_2) by fitting the experimental data via an effective medium approximation (EMA), as shown in Fig. 4(a) and 4(b) respectively. The change in the dielectric index is due to the thermal annealing, which clearly affects the scattering spectra. The change of imaginary part leads to a strong resonance, as shown in Fig. 2(c), whereas the change of real part leads to a blue shift of the resonance, as shown in Fig. 2(d). Both changes also influence the optical response that finally improves the SERS enhancement. This can lead to an average SERS enhancement of about a factor of 4 compared to the unannealed sample.Knowing that thermal annealing also enhances the SERS signals due to the lower ohmic damping of the plasmon resonance.

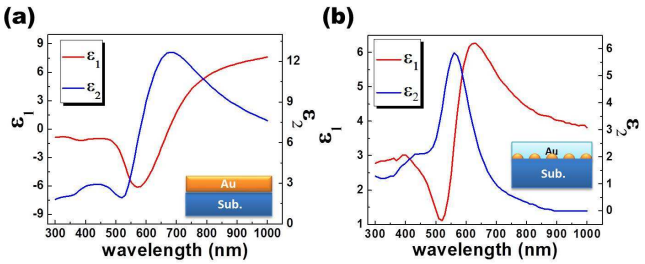

Fig. 4. Dielectric index (ε_1, ε_2) of (a) unannealed sample (b) the annealed sample.

Numerical Simulation Results

Numerical simulations based on rigorous coupled-wave analysis (RCWA) and finite difference time domain (FDTD) were carried out for two cases. The first case is a free standing gold nanosphere of 10 nm radius that is placed on a glass substrate, as shown in Fig. 5(b). The second case is an embedded gold nanosphere in the glass substrate, as shown in Fig. 5(c). We use (37 × 37) plane-waves in the xy-plane and 20 slices vertically to resolve the curved boundaries of the gold nanosphere. We choose a pitch size of 22 nm, which is comparable to the average particle spacing as shown in Fig. 1. Fig. 5(a) shows that the partially-embedded gold nanoparticle (AuNP) in glass has stronger reflectance compared to the exposed AuNP on glass. Fig. 5(b)-5(c) show the near field distribution for magnetic field $|H_y|$ of the free-standing and partially-embedded gold nanosphere. These figures illustrate that the larger index contrast for the embedded gold nanosphere in glass between the surrounding medium and the gold below the plasmon frequency leads to a stronger field confinement for the partially-embedded nanosphere compared to the free-standing case. The FDTD numerical simulation results and the enhancement factor evaluation due to optical field are in good agreement with the RCWA numerical simulation results (with the FDTD field strength slightly higher than RWA by a factor 1.13).

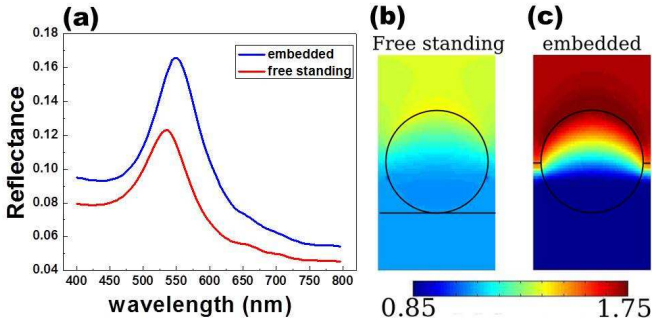

Fig. 5(a) Reflectance of the free standing gold nanosphere on glass and the partially embedded AuNP in the glass for normal incidence. (b) Magnetic field $|H_y|$ distribution at the center of the gold nanoparticle on glass (x-z plane) (c) Magnetic field $|H_y|$ distribution at the centre of the gold nanoparticle on glass (x-z plane).

SERS spectra were acquired by using a Raman spectrometer (Horiba LabRAM-HR800). A 632.8 nm HeNe laser with a maximum power of 20 mW was used for excitation. LabSpec

software was used to control the spectrometer and acquire process, and display data. The magnification of the objective lens was (100×). Because SERS effect arises from the close-packed AuNIs, generally, at the surface and gaps among the distributed partially embedded AuNIs that produce many hot spots, which are important for the SERS signal. Practically, careful optical focusing at the surface of the embedded AuNIs where the molecules are already adsorbed is very important for optimizing the SERS signal.

Fig. 6(a) shows the SERS spectra of p-MBA adsorbed on different prepared gold nanoislands samples of different initial thickness of gold films and gold nanoislands with optimized focus condition. The prepared samples were immersed in a 0.1ml of p-MBA to adsorb p-MBA molecules on the gold nanoislands. Then the SERS spectra of p-MBA molecules adsorbed on gold nanoislands of different samples were acquired. When the chemical bonds are formed, the peaks as shown in Fig. 6(a) can be attributed to p-MBA molecules. The strong peak at (1585 cm^{-1}) is due to the ν8a aromatic-ring vibrations and the peak at (1076 cm^{-1}) is due to the ν12 aromatic-ring vibrations, which are related to the C-S stretching characteristics. The peaks at (840 cm^{-1}) and (1422 cm^{-1}) show the presence of δ(COO −) and νs(COO −), respectively. The peak at (1021 cm^{-1}) is due to the characteristic of mono-substituted benzene derivatives.[23]

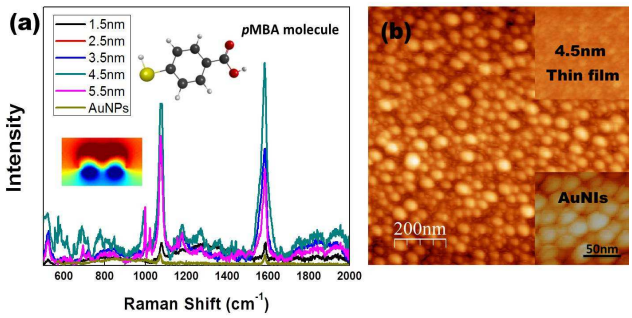

Fig. 6. (a) SERS spectra of thermally annealed gold thin films with various initial gold thicknesses. (b) AFM image of thermally annealed gold sample with initial thickness 4.5nm.

The intensity of the ν8a peak at (1585 cm^{-1}) was used to estimate the enhancement factor (EF) by using the following expression: $EF = (I_S/I_R)(N_R/N_S)$, where I_R and I_S denote the corresponding normal Raman and SERS intensities; while N_R and N_S denote the number of probe molecules which contribute to the normal and SERS signals. The molecular weight of p-MBA is 154.19 g/mol, the density of p-MBA ~1.4 g/cm^3, and the surface layer density of p-MBA on gold used ~0.5 $nmol/cm^2$.[24] Therefore, the highest EF value is about 3.4×10^7 (with $N_R/N_S \sim 3.4\times10^4$ and $I_S/I_R \sim 10^3$) for the prepared sample with initial gold thickness 4.5nm, as shown in Fig. 6.

Rhodamine 6G (R6G), dye molecule, was also used as probe molecules for the SERS measurements to assess the prepared SERS substrate. Raman scattering spectra were acquired and observed at different prepared samples and R6G concentrations, as shown in Fig.7. Raman peak positions at (612, 772, 1182, 1572, and 1647 cm^{-1}) were observed. The main peaks were located at (1310, 1363, and 1510 cm^{-1}) due to the stretching vibrations, and they agree well to those of the R6G Raman spectra reported previously.[25] Due to the molecular weight of R6G is (479.02 g/mol), the density is (0.79 g/cm^3), and the surface layer density of R6G is (~ 8.73×10^{-22} $mol/\mu m^2$)[26] the enhancement factor of the 1363 cm^{-1} band of R6G was estimated as large as 3.7×10^9 (with $N_R/N_S \sim 3.8\times10^6$).

Also, the Raman spectra of R6G adsorbed on the partially embedded AuNIs with initial gold thickness (4.5nm) were measured at different concentrations (1 nM, 10nM, 100nM, and 1 μM) of R6G with optimized focus condition. Increasing the concentration from 1 nM to 1 μM, leads to clear changes in the Raman spectra, as shown in Fig. 7(b).

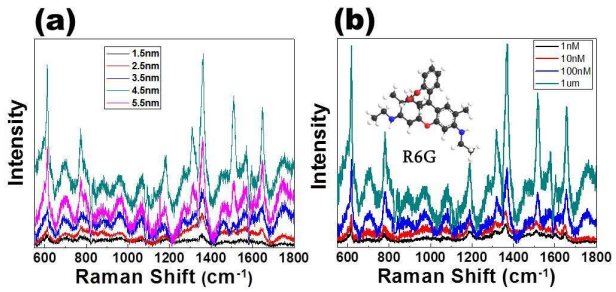

Fig. 7. (a) SERS spectra of R6G adsorbed on the partially embedded AuNIs with various initial gold thicknesses. (b) SERS spectra of R6G adsorbed on the partially embedded AuNIs with initial gold thickness 4.5nm for various R6G concentrations.

Based on RCWA and FDTD, we estimate the enhancement factor due to optical field by assuming $(EF)_{op}=\langle|E_S(r)|^4\rangle/|E_0|^4$, where $E_S(r)$ is the near-field on the exposed surface of AuNP and the brackets < > denote the average over the exposed AuNP surface. E_0 is the electric field on the substrate surface in the absence of AuNPs. For period arrays, we obtain $(EF)_{op}=4.9\times10^4$ (8.0×10^4) for partially-embedded AuNPs versus 2.4×10^4 (3.9×10^4) for fully exposed AuNPs with RCWA (FDTD) simulation. To take into the effect of randomness, we also performed FDTD calculation for a supercell consisting of nine randomly placed AuNPs in a unit cell with the same gap distance. We obtain an enhancement factor of 1.7×10^5 for partially-embedded AuNPs. The difference from experiment is attributed to chemical enhancement. For the prepared samples, the maximum SERS intensity was obtained for the sample with 4.5nm initial thickness of gold film. As shown in the AFM image, the size of the nanoislands is more uniform and the gap distance between Au NPs is very small, which help enhance the field. For the gold thin film with an initial thickness smaller than 3.5 nm, the gold nanoislands are small and diluted. Therefore, the field enhancement is not strong enough. On the other hand, for a thicker initial gold film larger than 5nm, the gold nanoislands become bigger with a small change in the surface morphology and the field enhancement is weak. However, it was shown that this prepared substrate of

embedded gold nanoislands in a transparent substrate is very stable. Thus a low-cost substrate can be prepared as large as needed without difficult fabrication techniques.

Conclusions

In this work, we present a low-cost, stable and sensitive SERS substrate based on partially-embedded gold nanoislands in a glass substrate. Partially embedded gold nanoislands were prepared by thermal annealing of gold thin films deposited on a glass substrate at a temperature close to the glass transition temperature of the substrate. Later, the prepared samples were optically characterized by using UV-Vis spectrophotometer to measure absorption spectra at different thickness of gold films. It is shown that absorption spectrum depends on the size and density of gold nanoislands. In addition, the spectroscopic ellipsometry was used to investigate the sample before and after annealing to show the LSPR response of this structure. The SERS intensity was measured for different samples at different thickness of gold films. It was shown that 4.5nm initial gold thin film sample has the highest SERS signal. The proposed SERS substrate is non-destructive, reproducible with high sensitivity, low cost, and easy to fabricate. This might make it feasible for biosensing applications.

Acknowledgements

This work was supported in part by the National Science Council of Taiwan under Contract No. NSC 01-2112-M-001-024-MY3.

Notes and references

1 R. Elghanian, J.J. Storhoff, R.C. Mucic, R.L. Letsinger and C.A. Mirkin, *Science,*1997,**277**,1078–1081.
2 M.Fleischmann, P.J.Hendra and A.J.McQuillan, *Chemical Physics Letters*,1973, **26 (2)**,163–166.
3 D.L. Jeanmaire, R.P. Van Duyne, *J. Electroanal. Chem*.,1977 ,**84**,1–20.
4 Alan Campion and Patanjali Kambhampati,*Chem.Soc.Rev.,* ,1998,**27**,241-250.
5 J. A. Dieringer, A. D. McFarland, N. C. Shah, D. A. Stuart, A. V. Whitney, C. R. Yonzon, M. A. Young, X. Zhang, and R. P. Van Duyne, *Faraday Discuss.*,2006,**132**,9–26.
6 Surbhi Lal, Stephan Link ,and Naomi J. Halas, *Nat. Photonics*, 2007, **1**, 641-648.
7 Shuming Nie and Steven R. Emory, *Science*,1997,**275**,1102 1106.
8 Ormonde AD, Hicks EC, Castillo J, Van Duyne RP., *Langmuir*,2004,**20**,6927-31.
9 Q. Yu, P. Guan, D. Qin, G. Golden, and P. M. Wallace, *Nano Lett.,*2008,**8**,1923–1928.
10 Nahla A Abu Hatab, Jenny M Oran, Michael J Sepaniak, *ACS Nano*,2008,**2**,377–385.
11 Richard J. C. Brown and Martin J. T. Milton, *J.Raman Spectrosc.*, 2008,**39**,1313–1326.
12 J. B. Jackson and N. J. Halas,*PNAS*, 2004,**101**,17930–17935.
13 Lianming Tong, Maurizio Righini, Maria Ujue Gonzalez, Romain Quidant and Mikael Käll, *Lab on Chip*,2009,**9**,93-195.
14 S. Foteinopoulou, J. P. Vigneron, and C. Vandenbem ,*Optics Express*,2007,**15**,4253-4267.
15 Anne Simo , Jörg Polte , Norbert Pfänder , Ulla Vainio , Franziska Emmerling , and Klaus Rademann, *J.Am. Chem. Soc.,*2012,**134** ,18824–18833.
16 Ya Chen, J. J. Jaakola, Antti S¨ayn¨ atjoki, Ari Tervonen and Seppo Honkanen, *J. Raman Spectrosc.,*2011,**42**,936–940.
17 M. Dubiel, H. Hofmeister , E. Wendler, *Journal of Non-Crystalline Solids*,2008,**354**,607–611.
18 E. Enrı´quez, M. A. Garcia, N. Carmona,J. F. Ferna´ndez, M. A. de la Rubia, *J Sol-Gel Sci Technol.,*2012,**62**,324–332.
19 H Krishna, R Sachan, J Strader, C Favazza, M Khenner and R Kalyanaraman, *Nanotechnology*,2010,**21**,155601.
20 R. S. Moirangthem, M. T. Yaseen, P.-K. Wei, J. Y. Cheng, and Y. C. Chang, *Bio Opt. Exp*.,2012,**3**,899-910.
21 M. G. Moharam and T. K. Gaylord, *J. Opt. Soc. Am*., 1981 **71(7)**, 811-818.
22 Allen Taflove and Susan C. Hagness, 2005,3rd ed., *Artech House Publishers*. ISBN 1-58053-832-0.
23 A. Michota and J. Bukowska, *J. Raman Spectrosc.*,2003,**34**, 21–25.
24 Yu Liu, Shuping Xu, Haibo Li, Xiaoguang Jian and Weiqing Xu, *Chem. Commun.,*2011,**47**,3784–3786.
25 Peter Hildebrandt and Manfred Stockburger, *J. Phys. Chem.* 1984,**88**, 5935-5944.
26 Wen-Lei Zhai, Da-Wei Li, Lu-Lu Qu, John S. Fossey and Yi-Tao Long, *Nanoscale*, 2012, **4**, 137–142.